Kirchhoff time-remigration and time-to-depth conversion – preliminary studies and possible applications

Alexandre de Souza Oliveira – ON/MCTI
Juarez Lourenço – ON/MCTI
Carlos A. S. Ferreira – ANP/RJ, currently at ANM/MT

This paper was prepared for presentation during the 18th International Congress of the Brazilian Geophysical Society held in Rio de Janeiro, Brazil, 16-19 October 2023.

Abstract

We report on the use of time-to-depth conversion after a time-remigration of seismic data. Our procedure is based on a Kirchhoff-type, isochrone-stack, integral operator. We have tested our algorithm on synthetic and real datasets. The real dataset used in this work is the public-domain Nankai Trough, available through the University of Hawaii. Using two velocity models (one accurate and other less accurate), we were able to successfully remigrate the Kirchhoff result using a less accurate velocity field, and convert it to depth via a direct time stretch of the time dimension.

Introduction

Prestack time-migration (usually Kirchhoff) is still a very usable imaging tool in situations in which lateral velocity variation is acceptable and/or subsurface geology is not so complex above imaging targets, structurally or physically speaking. When these assumptions are observed in a controlled way (i.e., a good knowledge of velocities and traveltimes), time-migration followed by a direct time-to-depth conversion by simply stretching the time axis into a depth axis may yield good imaging results, although systematic errors are always present (Black and Brzostowski, 1994). In this way, the image-ray concept (Hubral, 1977) may constitute a direct and succinct application, either using raytracing or simply via direct mapping.

Also it is known that in many exploration situations or even during appraisal times, when all imaging products are not already fully available to final interpretation purposes and/or deadlines are getting closer towards the choice of the site of a drilling well, quick procedures of depth imaging are common practice. This gives time-to-depth conversion a valuable and usable depth imaging status based on the necessities and limitations of information of a seismic dataset available to work with – i.e., when only 2D lines exist, instead of 3D interpretable volumes. This work is a study of a possible workflow towards depth imaging when one has limited data and too many targets to image.

Let us consider the fact that with the present procedure, when new velocity steps are available for processing, an remigrated output in the time domain is an immediate option, instead of a new migration run. And if this procedure is realized using a single step as depicted here, computational gains are immediate. The process is not free of non-uniqueness, since the most improved velocity model cannot be as equal to the least accurate model and this choice should serve as common sense to define the need for a new migration processing.

One of the advantages of working in the time domain concerns the use of RMS velocities for imaging or how the recorded wavefield extrapolation incorporates the velocity fields representative of subsurface rocks (Cunha and Rosa, 2001). In the time domain, for example, migration considers only the cumulative or average effect of the velocities of rocks traversed by the wave on its roundtrip path between the surface and several reflecting interfaces. Computationally, this means that traveltimes can be approximated by a double-square-root (DSR) equation, and in the case of finite offset each "branch" of the traveltime is associated with each one of these DSRs. Physically, using RMS velocities indicates that each branch of the traveltime only considers this constant average velocity to perform a stack along a diffraction curve and/or along an isochrone curve. Thus, everything works as if above the imaging (output) coordinate the medium were considered as homogeneous (constant velocity) (Cunha and Rosa, 2001). In principle, this allows one to use DSR formulas for constant velocity for the traveltime branches. For $v(z)$ medium, this is a straightforward relationship. Problems appear when lateral variation are present, which will give rise to time skewing and lateral shifts and formation of plumes (Black and Brzostowski, 1994; Bevc et al., 1995).

In this work we will show the results of time-remigration in some (simple and complex) 2D synthetic datasets and the result in one example of a real data (Nankai Trough). In those examples in which it is possible to convert the final image to the depth domain by a simple stretch of the time-migrated axis this will be directed assigned. On the other hand, in those models in which it is necessary to use image-ray tracing in order to perform the transformation, this will be suppressed, since currently we are working on this issue.

The most complex 2D synthetic model is physically representative of the pre-salt geology of the Brazilian offshore East Margin basin, composed of pre-salt, drift and open marine sedimentary sections over a basement ridge (Oliveira and Ferreira, 2009). The seismic data of this later model was realized separately and provided as direct input to the imaging procedures (migration and remigration), together with their respective velocity models, which were updated from the model used in Oliveira and Ferreira (2009) with the inclusion of lateral velocity variations. The

tests realized with synthetic data have shown that the procedures used in this work are kinematically accurate and reproduce final images similar to those directly migrated with more accurate velocities. As for the amplitudes, weighting functions already described in the literature were applied (e.g., Tygel et al., 1998; and Martins, 2001), whose main purpose is to treat the input amplitudes in a certain way so that geometrical-spreading factors are correctly transformed. The process can also be performed with amplitude preservation (Schleicher and Bagaini, 2003), when the same procedures do not alter the input amplitudes.

In the example using real seismic data, the existing velocity model was transformed to the time domain and one of its versions, transformed into a separate file, had its velocity values divided by a constant factor, giving rise to a velocity field distinct from the original. This procedure was carried out in order to have two different velocity models, validating the remigration procedure.

Method

Kirchhoff-type remigration theory

Kinematically discussed in Hubral at al. (1996b) and mathematically shown in Tygel et al. (1996), true-amplitude remigration is achieved by chaining weighted diffraction-stack migration and isochrone-stack demigration. In terms of reflection imaging, it represents one of the methods developed to solve specific imaging problems, the one that deals with "the updating of a *depth-migrated* seismic image according to a different or improved macrovelocity model" (Hubral et al., 1996a,b).

We have emphasized the word "*depth-migrated*" above mainly because, originally, the remigration problem in the context of the unified approach of Hubral and Tygel was developed considering the dual operations of diffraction and isochrone stacking, one performed in time and the other performed in the depth domain. This is an important observation, since in the chaining of the two true-amplitude imaging procedures – migration and demigration – one has to multiply their respective weight-functions, which do not depend on any reflector property, but are simulated using no other information than that provided by the given smooth macrovelocity model. Thus, a depth-related procedure. Our approach here for remigration, on the other way, is entirely performed in the time domain. Thus, it is a time-remigration. Also, we have reduced the procedure to the 2.5D domain (Martins, 2001), which is similar to other familiar 2.5D Kirchhoff-type imaging procedures that have already been published somewhere, like migration, DMO, OCO, MZO.

Hubral et al. (1996a) discusses time-remigration in the context of seismic image-waves, but restricted to the zero-offset domain and constant-velocity medium. To our knowledge, this is the only reference to time-remigration, besides the geometrical one in Schleicher et al. (1997) in constant-velocity medium using the Thales circle in the depth domain and its parabola counterpart in the time domain.

In the examples that follows a tilde symbol ("~") over functions and variables refer to the output model, including spatial positions, time coordinates and velocities. The remaining variables and functions without tildes refer to the input model, also including spatial positions, time coordinates and velocities. The input and output model both consider an arbitrary, single fold measurement configuration (i.e., sources and receivers are single pairs; see Tygel et al., 1996) of point sources and receivers distributed along the Earth surface, the location of them are described by a 2-D vector parameter, $\vec{\boldsymbol{\xi}} = (\xi_1, \xi_2)^T$. When referred freely, vector parameter $\vec{\boldsymbol{\xi}}$ varies in *A*, called migration aperture; or when referred specifically, as a stationary point, it determines an aperture constrained by an specific condition.

Stacking integral

Similar to the Kirchhoff-type theory described in Tygel et. al (1998) and Schleicher and Bagaini (2003), for each point $(\tilde{x}, \tilde{\tau})$ in the output time-remigrated section to be simulated, the stack result $\tilde{I}(\tilde{x}, \tilde{\tau})$ is obtained by a weighted stack of the input data, represented by the following integral

$$\tilde{I}(\tilde{x}, \tilde{\tau}) = \frac{1}{\sqrt{2\pi}} \int_A dx\, K_{RM}^{(2.5D)}(x; \tilde{x}, \tilde{\tau}) \partial_t^{\frac{1}{2}} I(x,t)|_{t=t_{RM}}(x; \tilde{x}, \tilde{\tau}), \quad (1)$$

where $I(x,t)$ is the input time-migrated (analytic) seismic section that is to be weighted by $K_{RM}^{(2.5D)}(x; \tilde{x}, \tilde{\tau})$ and then summed up along the stacking line or inplanat $t = t_{RM}(x; \tilde{x}, \tilde{\tau})$ (Tygel et. al, 1996). Both functions are dependent on the point $(\tilde{x}, \tilde{\tau})$ where the stack is to be placed, and on the variable x that specifies the location of the traces being summed in the stack. Moreover, *A* denotes the (spatial limited) aperture of the stack, the range of midpoints (in a common-offset gather) available in the time-migrated input section, $I(x,t)$. Finally, the time-reverse half-derivative

$$\partial_{-t}^{1/2}[f(t)] = \frac{1}{\sqrt{2\pi}} \int_{-\infty}^{+\infty} |\omega|^{\frac{1}{2}} e^{-i\frac{\pi}{4} sign(\omega)} F(\omega) e^{-i\omega t} d\omega \quad (2)$$

is applied in order to correct the pulse shape. In 2.5D this is a counterpart to the full 3D Kirchhoff-type migration (Bleistein et al., 1987; Schleicher et al., 1993).The stacking line $t = t_{RM}(x; \tilde{x}, \tilde{\tau})$ is defined by the kinematics of the operation, and the weight-function $K_{RM}^{(2.5D)}(x; \tilde{x}, \tilde{\tau})$ will be determined by the desired amplitude behaviour – true-amplitude and amplitude-preserving are the most common choices (Schleicher and Bagaini, 2003).

Stacking line

In constant-velocity medium and zero-offset configuration, Hubral et al. (1996a) derivated the following stacking line for the remigration problem as a Huygens image wave in the time domain

$$t = \sqrt{\tilde{\tau}^2 + \frac{4(x-\tilde{x})^2}{\tilde{v}^2 - v^2}}. \quad (3)$$

In the theory of velocity continuation of Fomel (2003), this is the analytic formula of the "wavefront" continuation or the summation path of the residual migration operator, augmented by a finite-offset term (not shown here). Here, $\tilde{v}^2$and v^2 are constant migration velocities in the output (time-remigrated) and input (time-migrated) domains, respectively. Eq. (3) was obtained as a special case of a *depth*-remigration, by simply substituting $z = vt/2$ and $\tilde{z} = \tilde{v}t/2$ in both domains. Viewed as a chaining of migration/demigration procedures, the depth counterpart

of Eq. (3) is obtained as the envelope of the ensemble of half-circle isochrones, which is the desired Huygens image wave at the instant of migration velocity v. Eq. (3) is not a traveltime, since there is no wavefield propagation, but only a stacking curve along an inplanat surface.

In inhomogeneous medium and considering the presence of mild lateral velocity variation, for a finite-offset (2*h*) configuration we have

$$t = \sqrt{\tilde{\tau}_D^2 - \frac{4h^2}{v_{RMS}^2}} \sqrt{1 - \frac{(x-\xi^*(\tilde{x}))^2}{(\frac{v_{RMS}^2}{4})\tilde{\tau}_D^2}}. \quad (4)$$

In (4), $\tilde{\tau}_D$ is the diffraction traveltime for coordinate $(\tilde{x}, \tilde{\tau})$ in the output space, represented by two DSRs for the two branches of the traveltime to the image point, where velocity $\tilde{v}_{RMS}$ is used relative for each source and geophone in that domain. Here, stationary value $\xi^*(\tilde{x})$ is the coordinate that relates the inplanat $t_{RM}(x; \tilde{x}, \tilde{\tau})$ with its respective coordinates in the input and output domains. Note that stacking line (4) is spatially constrained, both by the existence of the stationary coordinate $\xi^*(\tilde{x})$ and by the curvature of the inplanat (i.e.,v_{RMS}) in the input domain. These features will be commented below, when dealing with aperture issues. A complete geometrical explanation of this stationary condition is described in Tygel et al. (1996).

Weight-function

The final remigration weight-function is the product of 2.5D migration and demigration weight-functions (Tygel et al., 1996) that may also be expressed as in-plane and out-of-plane factors (Martins, 2001). Thus, in the time domain we consider, approximately:

$$K_{RM}^{(2.5D)}(x; \tilde{x}, \tilde{\tau}) = \frac{\sqrt{2}}{2} \frac{\tilde{\tau}}{v_{RMS}^{3/2}} \sqrt{\frac{1}{\tilde{t}_S} + \frac{1}{\tilde{t}_G}} \left(\frac{\tilde{t}_S}{\tilde{t}_G} + \frac{\tilde{t}_G}{\tilde{t}_S}\right) \frac{1}{(t_1+t_2)} \sqrt{\frac{1}{t_1} + \frac{1}{t_2}}, \quad (5)$$

where $\tilde{t}_S$ and $\tilde{t}_G$ are DSRs for source and receivers in the output domain for coordinate $(\tilde{x}, \tilde{\tau})$ and $\tilde{v}_{RMS}$, while t_1 and t_2 are DSR equations of the times (3) or (4). Dimensionally, this weight-function is expressed in [s$^{(1/2)}$/meters$^{(3/2)}$] units. Apart from the form of the weight-function in (5), a dimensionless stretch factor and a term regarding "local dip" at the reflector in the time domain may also be multiplied when referred. Other terms that may be multiplied in (5) are square roots of absolute values of determinants of Hessian matrices or, in 2.5D, curvatures of diffraction traveltimes for points in the input and output domains (Tygel et al., 1998; Martins, 2001).

Aperture

In (4), two conditions constrain the aperture range for time-remigration. The first is offset-dependent (i.e., $\tau_D^2 > 4h^2/v_{RMS}^2$), which means that in all offsets, very shallow to shallow events (whenever they are recorded) must be disregarded or are not imaged around any stationary value $\xi^*(\tilde{x})$ that may exist along these shallow time intervals. For the zero-offset situation, there is no constrain at all. The second constraint is related to the condition $(x - \xi^*(\tilde{x}))^2 < (\frac{v_{RMS}^2}{4})\tilde{\tau}_D^2$, which restricts the number of traces around the stationary value $\xi^*(\tilde{x})$. So far, in the following examples, we have used this criterion only in a very "ad hoc" way, depending on each case.

Examples

Synthetic data examples

We have tested our algorithm in two synthetic seismic datasets. Kirchhoff time-migration is used in all examples, unless otherwise stated.

Single reflector model – The first example represents a single interface of a syncline over a half-space. We have introduced a discontinuity in the form of a subvertical fault centered around distance 4.0 km in order to generate diffractions. The velocity of the layer over the interface is set to 2.5 km/s. We have modeled a common-offset section with 2*h* = 50 m. Model parameters are Nx = 400, Nz = 200, *dx* = *dz* = 25 m, while data parameters are N_{traces}=300, *dt* = 8 msec, where trace spacing equals to *dx* specified above, as well as source and geophone intervals. The seismic section of **Figure 1** depicts the modeled seismic section together with the typical bowtie pattern of reflections associated with this kind of model. In this example, a gradient of the order 0.03 Hz was included for lateral velocity variations.

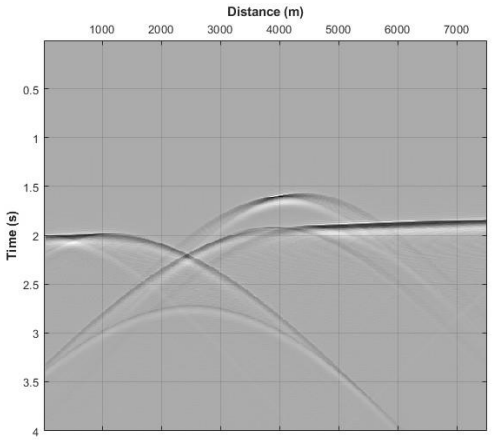

Figura 1 - Synthetic seismic data.

Presalt model – Our next synthetic example considers the previously model studied in Oliveira and Ferreira (2009), which describe the results of the modeling of a simple 2D seismic dataset acquired over a representative presalt model derived from any of the Brazil East margin offshore basins (**Figure 2**). The geologic model with its respective interval velocities is originally made of four sequences: (I) the basement (6.5 km/s); (II) the presalt section (4.5 km/s); (III) the salt layer (5.5 km/s); (IV) the Tertiary-Upper Cretaceous section, with a constant velocity gradient v(z). For the next example that follows, this model was updated to include lateral velocity variations in the Cretaceous section and in the sag/rift section.

Figure 3 depicts one common-offset section with 2*h* = 50 m. Again, the main features observed are good continuity of the flat and linear events, like the water line, the water bottom, parts of the bottom of the salt layer and the high of the basement and the ramp of the basement. But this time, due to lateral velocity variations in the sections commented above, some skewing of the reflections are also observed to the right of the section. Also it is evidente that due to the

presence of a lateral velocity variation, an “advance” in reflection recording introduces a “time-dip” along the whole section, a feature that must be “remedied” for interpretation purposes or serve as decision to a depth-miration Imaging (Black and Brzostowski, 1994).

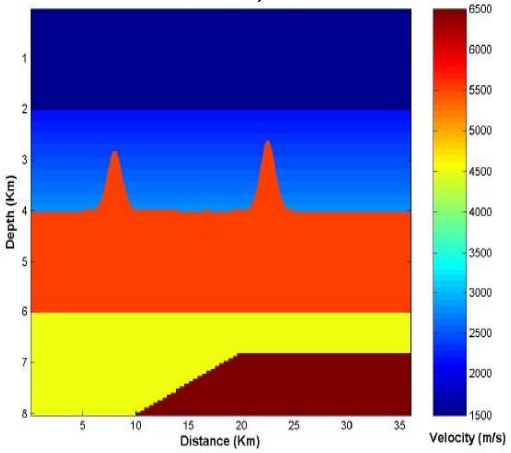

Figure 2 - Presalt depth velocity model (Oliveira and Ferreira, 2009).

In order to time-migrate the seismic section depicted in **Figure 3**, it was necessary to derive the RMS velocity field that were used to extrapolate the wavefield in the time domain. **Figure 4** is the time-domain equivalent of the depth velocity model seen in **Figure 2**. It is interesting to note in this model that since there is a lateral velocity variation in the sag/rift section, times to the top of the basement up to 10 km are faster than the ones over its ridge section.

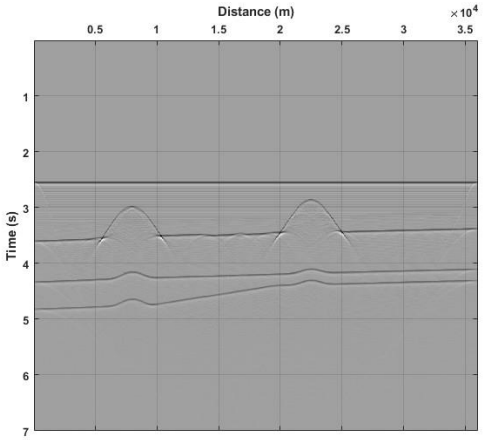

Figure 3 - Common-offset section (2*h* = 50 m) simulating a 2D seismic marine acquisition over the area of the velocity model in **Figure 2**.

Real data example – Nankai Trough

Published by Moore et al. (1990), the Nankai trough data considered here is a subset of a larger dataset and that is made available by the University of Hawaii for download. In Forel et al. (2005), this data is processed using CWP Seismic Unix tools, for didactical reasons. It is part of the 2D regional line NT62-8 (Moore et al., 1990), with CDP range 900-1300 (401 bins, sorted from 326 shots in the range 1687-2012, *dx* = 6.67 among bins) and *dt* = 4 msec (2750 time-samples or 11 seconds of record). **Figure 5** depicts the zero-offset section that was processed and stacked by Forel et al. (2005) and commented in their primer guidelines.

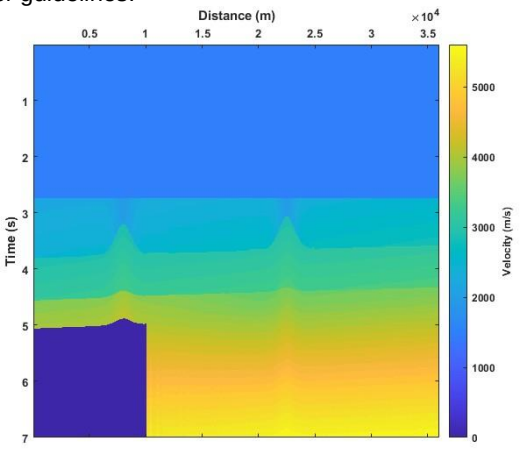

Figure 4 – Velocity model in the time domain (RMS). Compare with **Figure 2**.

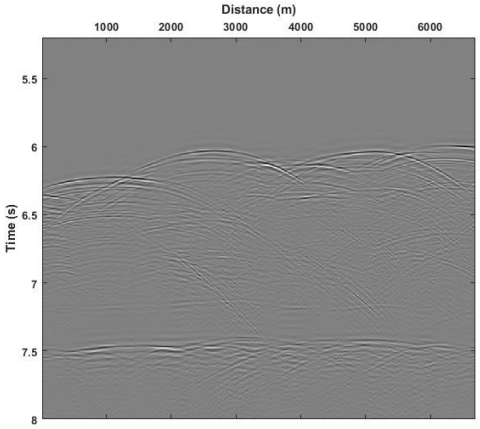

Figure 5 – Zero-offset section of the Nankai data. Line NT62-8 (Moore et al., 1990).

Results

Synthetic data examples

The seismic section of **Figure 1** was time-migrated using the true velocity 2.5 km/s and using a velocity set to 2.0 km/s, this latter in order to generate an input section to the remigration process. **Figure 6** depicts the two time-migrated sections. It is clear that when the wrong velocity is used the final image is not completely focused in time.

Figure 7 depicts two results: the first (top section) is the result of time-remigration of the time-migrated section depicted at the bottom of **Figure 6**. Clearly the remigration imaging was able to focus the latter section, which is equivalent to the top section of **Figure 6**.

The second result in **Figure 7** (bottom) is the time-to-depth conversion, obtained directly by simply stretching the time axis to depth. Since this is a simple example, using a single

velocity, the transformation was able to correctly map the reflector from time to depth.

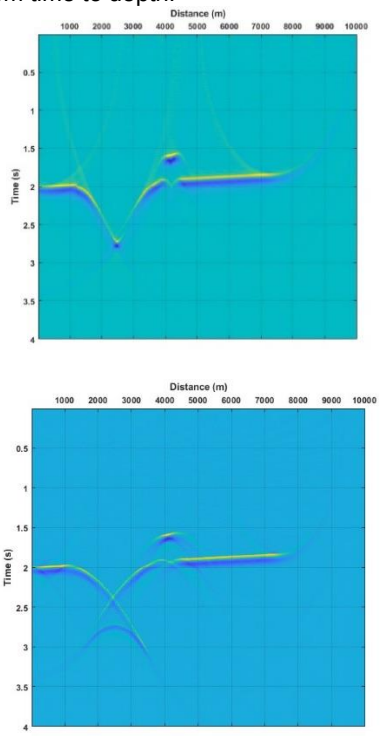

Figure 6 – Comparison of Kirchhoff time-migrated sections: right velocity (above) and wrong velocity (below).

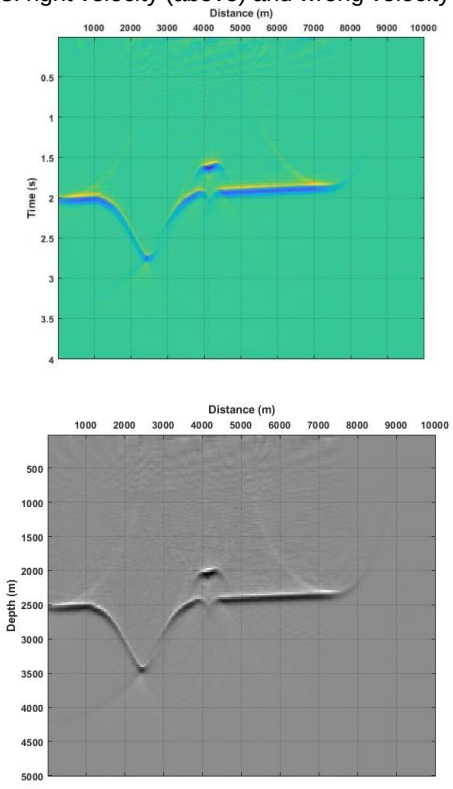

Figure 7 – *Top*: Kirchhoff time-remigrated section of **Figure 6** (bottom). *Bottom*: time-to-depth conversion of the tme-remigrated section (top).

Finally, in **Figure 8** and **Figure 9** it is depicted the processes of Kirchhoff migration and remigration for the presalt model common-offset section of **Figure 3**. For this example, a Ormsby passband filter was first applied to the input section of **Figure 3** in order to suppress high-frequency numerical noise.

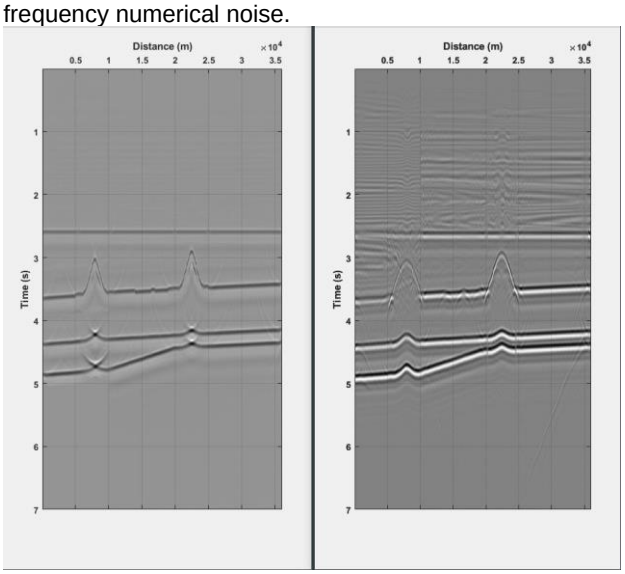

Figure 8 – Kirchhoff time-migration for the common-offset section in **Figure 3**. *Left*: accurate velocity result. *Right*: under-migrated result.

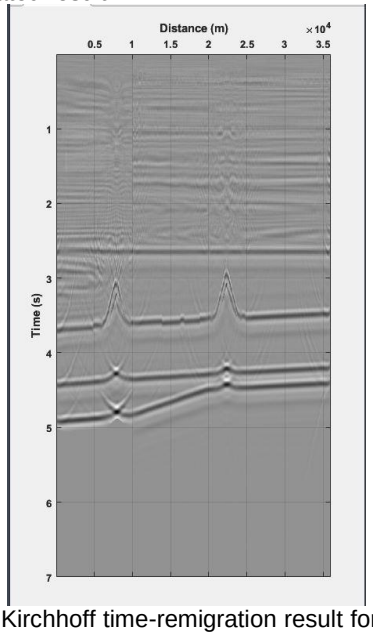

Figure 9 – Kirchhoff time-remigration result for the under-migrated section of **Figure 8** (right panel). Compare it with the section in the same figure (left panel).

Real data example – Nankai Trough

For processing purposes (Forel et al., 2005), this dataset was first resampled from 2 msec to 4 msec, and anti-alias filtered using 16-21-85-95 Hz as threshold in order to avoid frequency-folding beyond Nyquist. Due to its nature of being a seismic data obtained over deep waters, the recorded reflections show little moveout, which represents a challenge to seismic processing and velocity picking via semblance analysis. Also, the input data was previously

corrected for spherical divergence using an exponent power $t^{2.21}$ as gain function (Forel et al., 2005).

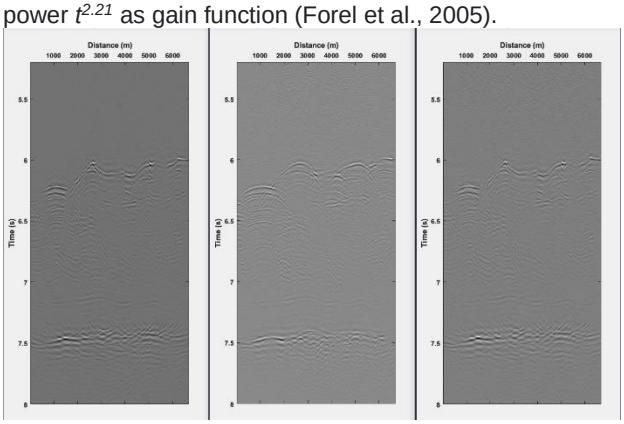

Figure 9 – Comparison of Kirchhoff results for the Nankai data: time-migrated (*left*); under-migrated (*center*); and time-remigrated (*right*).

In **Figure 9** we show the results of Kirchhoff time-migration (migrated and under-migrated) (left and center panels), and the remigration result (right panel) for the seismic section of **Figure 5**. Note that at the dècollement level (around 7.5 s) the presence of migration smiles indicates higher velocity values (over-migration). In fact, in Forel et. al (2005) it was suggested that the current velocity model available for download for this example should be adequately updated.

Conclusions

We have tested a Kirchhoff time-remigration process in synthetic and real datasets. The main synthetic dataset is the one previously studied in Oliveira and Ferreira (2009), which is physically representative of the presalt geology of the Brazilian East Margin basins, updated to include lateral velocity variations. The real dataset is a zero-offset subset of the Nankai data published by Moore et al. (1990) and reprocessed in Forel et al. (2005) for didactical reasons.

The tests carried out so far showed that the result of remigration depends on the quality of the input section (i.e., sub-migrated section). This includes resolution, noise content and an effective QC eventually realized (e.g., mainly frequency filtering).

Intrinsic time migration errors (see Black and Brzostowski, 1994) were considered in this work, but not commented or corrected with any "remedy". Further time-to-depth conversion should accommodate or minimize such systematic errors or even others methodologies.

The article addresses both the kinematics (i.e., traveltimes) and the dynamics (weight-functions and amplitudes) of imaging by remigration, but greater emphasis is put on the kinematic imaging results only, for comparison reasons. The dynamic aspects will be considered in future works somewhere by the first author.

Acknowledgments

The first author would like to thank CNPQ for his MSc scholarship, during all the stages of this research. The third author would like to thank ANP/RJ and ANM/MT for the permission to take part in this work.

References

Black, J. L.; Brzostowski, M. A., 1994, Systematics of time-migration errors: *Geophysics*, **59**, 1419-1434.

Bevc, D.; Black, J. L.; Palacharla, G., 1995**.** Plumes: Response of time migration to lateral velocity variation. *Geophysics*, 60, 1118-1127.

Cunha, C. A.; Rosa, A. R., 2001. Deepening the use of time migration. 7th Congresso of Brazilian Geophys. Soc.

Bleistein, N.; Cohen, J. K.; Hagin, F. G., 1987. Two-and-one-half dimensional Born inversion with na arbitrary reference. *Geophysics*, **52**, 26-36.

Fomel, S., 2003. Velocity continuation and anatomy of residual prestack time migration. *Geophysics*, **68**, 1662-1672.

Forel, D.; Benz, T.; Penning, T., 2005. Seismic data processing with SU: A 2D seismic data processing primer. Society of Exploration Geophysicists.

Hubral, P., 1977, Time migration: Some ray theoretical aspects: *Geophys. Prosp.*, **25**, 738-745.

Hubral, P.; Tygel, M.; Schleicher, J., 1996a. Seismic image waves. *Geophysics J. Int.*, **125**, 431-442.

Hubral, P., Schleicher, J. & Tygel, M., 1996b. A unified approach to 3-D seismic reflection imaging-Part I: Basic concepts, *Geophysics*, **61**, 742-758.

Martins, J. L., 2001. Migração, demigração e imageamento em 2.5D com inclusão de alguns casos analíticos. Tese de doutorado (in Portuguese). Unicamp/SP, 107p.

Moore, G. F.; Shipley, T. H.; Stoffa, P.; Karig, D. E.; Taira, A.; Kuramoto, S.; Tokuyama, H; Suyehiro, K., 1990. Structure of the Nankai Trough accretionary zone from multichannel seismic reflection data. *J. Geophys. Res*., **95**, 8753-8765.

Oliveira, A. S.; Ferreira, C. A. S., 2009. Modeling of a synthetic presalt 2D seismic dataset representative of offshore East margin basins (Brazil) – preliminary results. 11th Int. Congress of the Brazilian Geophys. Soc.

Schleicher, J.; Tygel, M.; Hubral, P., 1993. 3D true-amplitude finite-offset migration. *Geophysics*, **58**, 1112-1126.

Schleicher, J.; Hubral, P.; Hoecht, G.; Liptow, F., 1997. Seismic constant-velocity remigration. *Geophysics*, **62**, 589-597.

Schleicher, J.; Bagaini, C., 2003. Controlling Amplitudes in 2.5D common-shot migration to zero offset. Wave Inversion Technology.

Tygel, M., Schleicher, 3. & Hubral, P., 1996. A unified approach to 3-D seismic reflection imaging-Part IT: Theory, *Geophysics*, **61**, 759-775.

Tygel, M.; Schleicher, J.; Hubral, P.; Santos, L. T., 1998. 2.5D true-amplitude Kirchhoff migration to zero-offset in laterally inhomogeneous media. *Geophysics*, 63, 557-573.